Multiwall Nanotubes Can Be Stronger than Single Wall Nanotubes and Implications for Nanocomposite Design

E. M. Byrne,[1,3,4] M. A. McCarthy,[1,3,4,5] Z. Xia,[2] and W. A. Curtin[3]

[1]*Department of Mechanical and Aeronautical Engineering, University of Limerick, Limerick, Ireland*
[2]*Department of Mechanical Engineering, University of Akron, Akron, Ohio 44325, USA*
[3]*Division of Engineering, Brown University, Providence, Rhode Island 02912, USA*
[4]*Composites Research Centre, University of Limerick, Ireland*
[5]*Materials and Surface Science Institute, University of Limerick, Limerick, Ireland*

(Received 14 December 2008; published 24 July 2009)

Molecular dynamics modeling shows that multiwall carbon nanotubes (MWCNTs) with sp^3 interwall bonding have strengths exceeding those of single-wall carbon nanotubes (SWCNTs) containing the same size initial intrawall defect, and are far less sensitive to defect size. Thus, although processing methods used to increase interwall coupling also create intrawall defects, analyses here show that the strengthening effects and enhanced load transfer compensate for the creation of defects and make MWCNTs with interwall bonding preferable to SWCNTs as mechanical reinforcements in composites. These results are consistent with new experimental data and suggest a new design methodology for CNT-based composites.

DOI: 10.1103/PhysRevLett.103.045502 PACS numbers: 62.25.Mn, 61.48.De, 62.23.Pq

The use of carbon nanotubes to reinforce polymer, ceramic, and metal matrices to achieve enhanced stiffness, strength, and toughness, in a wide array of applications has exploded in the last several years [1–10]. Single-wall carbon nanotubes (SWCNTs) appear ideal, with theoretical tensile strengths approaching 100 GPa [11–14]. But, like most brittle materials, SWCNTs contain fabrication defects that lower their strengths below the ideal level [15,16]. In many applications, multiwall CNTs (MWCNTs) have been used due to their lower cost, availability, and ease of fabrication [4,7–10]. MWCNTs have the possibility of interwall coupling between the graphitic CNT walls [17–21]. Molecular dynamics (MD) models show that interwall coupling improves interwall shear strength and load transfer [21–24] and compression buckling resistance [24]. Calculations also predict the presence of strength-reducing intrawall defects [13,14,25–27]. However, MWCNTs grown by chemical vapor deposition (CVD), which should contain a high level of defects, have strengths greater than either SWCNTs or MWCNTs grown by arc discharge, and the strengthening is attributed to interwall coupling [28,29]. Recent experiments by Peng *et al.* [30] clearly showed that the outer wall of an uncoupled MWCNT can have similar strength to that of a SWCNT with small defects and that irradiating MWCNTs induces interwall coupling that leads to much higher load-carrying capacity with little loss of strength. In spite of significant experimental efforts to measure strengths of MWCNTs [28,31,32], no modeling work to date has investigated MWCNT tensile strength.

Here, we show via simulation that MWCNTs with sp^3 interwall bonding have strengths exceeding those of SWCNTs containing the same size initial intrawall defect. Increasing interwall bonding also causes planar fracture rather than ''sword-and-sheath'' fracture. We further argue that MWCNTs with sufficient interwall bonding should have a minimum strength of 35–45 GPa. These results are consistent with the new experimental data [30]. The strengthening effects of interwall bonding can compensate for the creation of defects during irradiation, so that MWCNTs with interwall bonding can be preferable to even the smallest and strongest SWCNTs for use as mechanical reinforcements in composites.

Molecular dynamics (MD) was used to simulate nanotube failure [12–14,21–24]. We study (50,0) single-wall CNTs (diameter = 4 nm), $(50, 0)/(41, 0)$ double-wall CNTs (DWCNTs) [Fig. 1] and $(59, 0)/(50, 0)/(41, 0)$ triple-wall CNTs (TWCNTs), of length 11.8 nm, sufficient to preclude end effects. DWCNTs and TWCNTs were populated with randomly-distributed interwall sp^3 bonding of variable density (number of sp^3 bonds between walls divided by average number of atoms in the two walls) [33]. Crack-like defects were introduced at the middle cross section of the (50,0) wall by removing hexagonal units of carbon in a horizontal line [14]. Defect length is defined as the distance between the intact C-C bonds on either end of the defect. Hydrogen atoms saturate the dangling bonds, as expected for MWCNTs grown by CVD.

The Tersoff-Brenner potential [34] with a modified cutoff to improve bond breaking [35] was used, with a Lennard-Jones model for nonbonded interwall interactions [36,37] connected to the bonding potential via cubic splines. This potential underestimates nanotube strength compared to quantum calculations [14], but absolute strengths are not crucial to our major conclusions. Nanotubes were relaxed for 18.75 ps at $T = 0.5$ K using a Berendsen thermostat [38] and a 0.25 fs time step. Loading was applied by fixing the z displacements of the bottom two rings of C atoms and displacing the top two rings vertically by 0.025 Å every 0.25 ps. Total force was

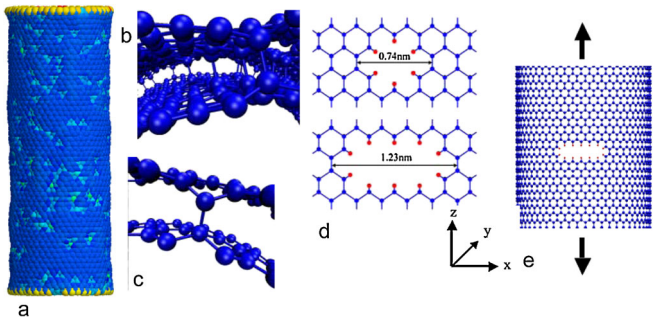

FIG. 1 (color online). Schematic of computational models: (a) Entire DWCNT with interwall sp^3 bonding, showing distortions of the wall surface and the atomic energy variations due to sp^3 bonds; (b),(c) Views of the DWCNT along the tube axis, showing the interwall bonding and local distortion in the CNT structure; (d) Examples of small defects placed into the outer-wall; (e) SWCNT (50,0) with a 1.72 nm defect perpendicular to the loading axis.

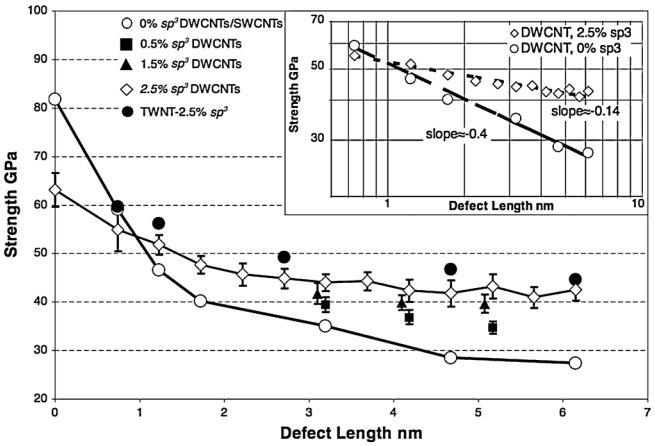

FIG. 2. SWCNT and MWCNT strengths vs initial defect (crack) length, for varying densities of interwall sp^3 bonding. For defects longer than ≈ 1 nm, the MWCNTs with interwall sp^3 bonding are stronger than SWCNTs or MWCNTs with no interwall bonding. Inset shows approximate power-law scaling of strength versus length, $\sigma \propto c^{-\beta}$, with MWCNTs with interwall bonding showing weak scaling (small β).

divided by CNT cross-sectional area $A_{\text{cnt}} = \pi[(r_0 + 0.5t)^2 - (r_i - 0.5t)^2]$ to obtain the stress, where r_o and r_i are the outer and inner radii, and $t = 0.335$ nm is interwall spacing. Use of A_{cnt} allows for consistency among SWCNTs and MWCNTs. For each crack size, 5–10 random sp^3 bond distributions were simulated.

Figure 2 shows the strength versus defect size and nanotube structure. For SWCNTs and DWCNTs with no interwall bonding, the defect-free strength is 82 GPa (as in [14]). Strength decreases with increasing defect size as $\sigma \propto c^{-\beta}$, $\beta \approx 0.4$ (Fig. 2, inset), close to the value $\beta \approx 0.5$ predicted by fracture mechanics for a sharp crack in a brittle material. DWCNTs with 2.5% sp^3 interwall bonding show entirely different strength scaling (Fig. 2 and inset), decreasing slowly with increasing defect size as $\sigma \propto c^{-\beta}$, $\beta \approx 0.14$. With no defects, these tubes are weaker than SWCNTs due to disorder induced by sp^3 bonds (Fig. 1) but with defects larger than 1 nm the strength is larger than that for a SWCNT. The weak scaling shows that DWCNTs are *toughened* by sp^3 bonding. The inner wall constrains the opening of the outer wall crack via stretching of interwall bonds, decreasing the crack-tip stresses and being more effective for larger defects, thus decreasing the scaling exponent. This mechanism is similar to the strengthening of a thin brittle film on a tough elastic substrate [39]. Strengths of TWCNTs with 2.5% sp^3 bonds are even larger because the outer wall provides additional constraint. Figure 2 also shows the strengths for DWCNTs with 0.5% and 1.5% sp^3 bond fractions; strengths are reduced relative to the 2.5% case because of the weaker mechanical constraint. However, the DWCNT strength is larger than the SWCNT strength. With this mechanistic insight, we conclude that the MWCNT strength is higher than that for SWCNTs, and can be *insensitive* to defect size for sizes beyond one or two vacancies. This is the first main result of this Letter.

A lower bound for strengths of MWCNTs with interwall bonding can be estimated. For high interwall bonding in a many-walled CNT, failure of the outer wall at $\bar{\sigma}$ increases the stress on the inner neighbor to $1.5\bar{\sigma}$ [40]. This suggests a minimum MWCNT strength of $\sigma_{\text{min}} \approx \sigma_o/1.5$ where σ_0 is the defect-free strength. With $\sigma_0 \approx 63$ GPa (Fig. 2), we find the value $\sigma_{\text{min}} \approx 42$ GPa that is within 5% of our simulation data on TWCNTs and 5%–10% of our data for 1.5% and 2.5% DWCNTs. This estimate ignores "weak-link" size effects [41] but shows that strengths for MWCNTs with many walls should exceed those of SWCNTs with defects larger than 1.7 nm.

The fracture mode changes with sp^3 density. For high sp^3 bonding [2.5%; Fig. 3(a)], a high stress concentration occurs in the neighboring wall, resulting in near-planar fracture. Low sp^3 bonding [0.5%; Fig. 3(b)] increases the length over which stress is transferred among walls, such that the inner wall fails at a slightly weaker location away from the outer wall fracture plane, leading to the "sword-and-sheath" failure mode. For intermediate sp^3 bonding (1.5%), the failure mode varies depending on the sp^3 bond distribution. A TWCNT can show features of both modes as well [Fig. 3(c)]. This transition in fracture mode is consistent with experimental observations [28–30] and is the second main result of this Letter.

We now compare our results to recent experimental data [30]. The first six columns in Table I present the data published by Peng *et al.* on six specific MWCNTs of varying diameters, exposed to varying degrees of irradiation, including the number of walls coupled by interwall bonding as measured after fracture. The number of load-bearing walls increases with increasing irradiation dose, because irradiation creates interwall bonding and at increasing depths into the MWCNT. The unirradiated samples (1,2,3) have no interwall bonding and thus fracture *as if* they were SWCNTs with an average strength of

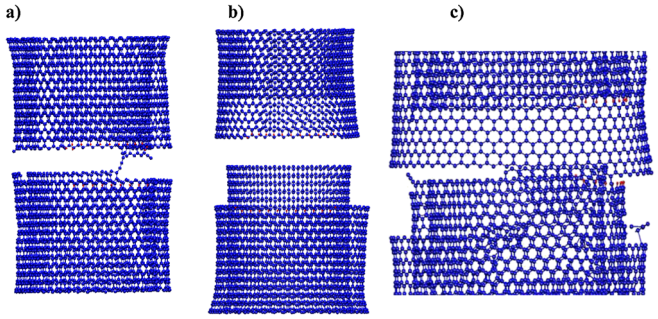

FIG. 3 (color online). Fracture Mode Transition: (a) Flat fracture mode in a DWCNT with 2.5% sp^3 interwall bonding; Carbon ''chains'' can often be seen linking the structure after failure; (b) Sword-and-sheath fracture mode in a DWCNT with 0.5% sp^3 bonding; (c) Mixed fracture in a TWCNT with 2.5% sp^3 bonding.

102 GPa corresponding reasonably to first-principles calculations of SWCNTs with single vacancies. The strength of a SWCNT with a single vacancy using the present potentials is 65 GPa [14,34]. The nanotube deformation is essentially elastic so a useful comparison between experiments and MD simulations is obtained by considering strength *ratios*. These ratios are calculated in Table I by dividing the experimental data by 102 GPa and our MD data by 65 GPa. Table I shows good agreement between experimental and simulation strength ratios except for Sample 6. This discrepancy suggests that the high irradiation for Sample 6 induces large defects correlated between successive walls, consistent with a greatly-reduced elastic modulus and evidence of amorphous carbon [30]. Our results are thus consistent with the quantitative data of Peng *et al.*; this is the third main result of this Letter.

We now examine some basic design concepts for use of MWCNTs in composites that are essential for making decisions on fundamental material design of nanocomposites for high strength. Nanocomposites may consist of aligned, partially-aligned or random CNTs, but tensile strength is generally controlled by the fraction of reinforcements within some angle of the tensile loading axis [42]. Thus, micromechanical theories for aligned fibers provide a guide for design of the CNT reinforcements. In a composite with aligned CNTs of outer diameter D, consider a volume fraction $V_{\rm cnt}$ of n-walled CNTs having nominal area $\frac{\pi}{4}(D+t)^2$. The composite ultimate tensile strength $\sigma_{\rm uts}$ is proportional to the *actual* load-bearing area fraction $V'_{\rm cnt} = [\frac{2t}{D}(\frac{1+n+(n^2-1)t/2D}{(1+t/D)^2})]V_{\rm cnt}$. For CNTs having a Weibull strength distribution with Weibull modulus m [43] and coupled to a matrix via interfacial shear strength τ, $\sigma_{\rm uts}$ can be accurately estimated using the ''global-load-sharing'' model [44] as

$$\sigma_{\rm uts} = V'_{\rm cnt}\varphi(m)\left[\frac{2\tau L}{\sigma_{\rm cnt}D}\right]^{(1/m+1)}\sigma_{\rm cnt}, \qquad (1)$$

where $\varphi(m) = (\frac{2}{m+2})^{(1/m+1)}\frac{m+1}{m+2}$ is a statistical ''bundle'' factor, $[\frac{2\tau L}{\sigma_{\rm cnt}D}]^{(1/m+1)}$ is a statistical length scaling factor, and $\sigma_{\rm cnt}$ is the reinforcement strength measured at gauge length L [44]. Equation (1) neglects the strength contribution of the matrix, which is small for polymers, ceramics, and most metals. The Weibull modulus, related to the coefficient of variation (COV) as $m \approx 1.2/{\rm COV}$, arises from a combination of the underlying Weibull distribution of defect sizes having Weibull modulus m' and the defect size-scaling exponent β, with $m = m'/\beta$. Thus, the low β for DWCNTs with interwall bonding increases the Weibull modulus by a factor of $0.4/0.14 \approx 3$ over SWCNTs with the same underlying defect distribution.

Within the above framework, the design trade-off is between very small diameter SWCNTs and larger n-wall MWCNTs with interwall coupling with the same $V_{\rm cnt}$ (i.e., the same total amount of carbon material or the same load-bearing area of carbon), the same interface τ, and the same underlying statistical defect distribution m'. To make comparisons as favorable as possible for SWCNTs, we compare MWCNT materials to SWCNTs of the *smallest* feasible diameters of $D_{\rm SW} = 1.1$ and 1.8 nm and the *highest* feasible strength of $\sigma_{\rm SW} = 100$ GPa. For specific results, we use the strengths from Peng *et al.* at $L = 2000$ nm, a value $\tau = 50$ MPa typical of polymer, metal, and ceramic matrices [44], and $m = 7$ typical of good-quality carbon fibers. Then, $\varphi(3m)/\varphi(m) = 1.16$ and $(2\tau L/\sigma_{\rm MW}D_{\rm MW})^{(1/3m+1)}/(2\tau L/\sigma_{\rm SW}D_{\rm SW})^{(1/m+1)} \sim 0.8$–$0.9$ for a wide range of $\sigma_{\rm MW}$ and $D_{\rm MW}$. Hence, the

TABLE I. Observed and predicted tensile strengths for six individual MWCNTs subjected to irradiation. Also shown is the strength ratio defined as the strength normalized to the strength of a SWCNT with a single vacancy defect; this scales out the absolute difference arising from the use of the interatomic potentials in the predictions. Samples 1–3 are essentially SWCNTs and thus serve as reference cases.

Sample	Outer Diam. (nm)[a]	# Walls coupled[a]	Dose (C cm^{-2})[a]	Measured Strength (GPa)[a]	Measured Strength Ratio[a]	Predicted Strength (GPa)	Predicted Strength Ratio
1,2,3	14.7–26.0	1	0	102 (ave)	1.0	≈ 65[b]	1.0
4	39.48	3	3.1	82	0.80	45–55	0.69–0.85
5	25.87	18	31.0	58	0.57	43	0.66
6	49.01	52	558.0	35	0.34	43	0.66

[a]Reference [30].
[b]Reference [14,34].

ratio of MWCNT and SWCNT composite strengths, $\sigma_{\mathrm{uts,MW}}/\sigma_{\mathrm{uts,SW}}$, is controlled mainly by $V'_{\mathrm{cnt}}/V_{\mathrm{cnt}}$, favoring MWCNTs, and $\sigma_{\mathrm{cnt,MW}}/\sigma_{\mathrm{cnt,SW}}$, favoring SWCNTs. Assuming that a given radiation dosage effectively couples n walls (e.g., Table I), we can maximize $\sigma_{\mathrm{uts,MW}}/\sigma_{\mathrm{uts,SW}}$ by using a fully dense MWCNT of diameter $D_{\mathrm{MW}} \sim 2(n+1)t$. For a dosage coupling $n = 3$ walls with $\sigma_{\mathrm{MW}} = 82$ GPa (e.g., Sample 4), $D_{\mathrm{MW}} = 2.4$ nm is optimal and yields $\sigma_{\mathrm{uts,MW}}/\sigma_{\mathrm{uts,SW}} = 0.92$–$1.32$; i.e., the MWCNT composite has 92%–132% of the strength of an equal nominal area of small, strong SWCNTs. For a dosage coupling $n = 18$ walls with $\sigma_{\mathrm{MW}} = 58$ GPa (e.g., Sample 5), $D_{\mathrm{MW}} = 12.5$ nm is optimal and yields $\sigma_{\mathrm{uts,MW}}/\sigma_{\mathrm{uts,SW}} = 0.61$–$0.87$. For a dosage coupling $n = 52$ walls with $\sigma_{\mathrm{MW}} = 35$ GPa (e.g., Sample 6), $D_{\mathrm{MW}} = 35$ nm is optimal and yields $\sigma_{\mathrm{uts,MW}}/\sigma_{\mathrm{uts,SW}} = 0.37$–$0.53$. MWCNT-based composites are thus competitive with the *best possible* SWCNT systems.

SWCNTs are brittle materials (Fig. 2) and so as-processed SWCNT strengths could be lower than 100 GPa. Functionalization of SWCNTs to achieve coupling to a matrix is also accompanied by strength decreases [45,46]. In contrast, our simulation results demonstrate that MWCNTs with interwall coupling are damage tolerant (strength weakly dependent on defect size) with high retained strengths unless exposed to harsh conditions. Considering reliability and robust design (as well as cost and manufacturability, issues not discussed here), we conclude that MWCNTs suitably designed using Eq. (1) are preferable to SWCNTs for high-performance materials. This is the fourth main result of this Letter.

In summary, we have shown that MWCNTs with interwall coupling are inherently stronger than SWCNTs with the same size initial intrawall defect, a result understood through basic mechanics considerations. We find that the measured and simulated strength ratios between irradiated MWCNTs and unirradiated SWCNTs are in reasonable agreement. We have then also shown that composites composed of MWCNTs can be as strong as composites composed of the highest-strength, smallest diameter SWCNTs, and conclude that composites with suitably-designed MWCNTs (diameter, number of walls, and irradiation dosage) can perform better than most SWCNT-based composites. In totality, our results provide a fundamental framework for guiding the creation of high-performance composites based on MWCNTs through carefully-controlled interwall bonding.

W. A. C. and Z. H. X. acknowledge support by NASA GRC 06- SSFW2-0043 and the Brown NSF MRSEC. E. M. B. gratefully acknowledges the support of Kildare County Council and U. Limerick.

[1] E. Flahaut *et al.*, Acta Mater. **48**, 3803 (2000).
[2] A. Peigney *et al.*, Chem. Phys. Lett. **352**, 20 (2002).
[3] G.-D. Zhan *et al.*, Nature Mater. **2**, 38 (2003).
[4] Z. Xia *et al.*, Acta Mater. **52**, 931 (2004).
[5] J. P. Fan *et al.*, Appl. Phys. Lett. **89**, 1 (2006).
[6] C. S. Goh *et al.*, Mater. Sci. Eng. A **423**, 153 (2006).
[7] Y. Shimizu *et al.*, Scr. Mater. **58**, 267 (2008).
[8] S. Pasupuleti *et al.*, Mater. Sci. Eng. A **491**, 224 (2008).
[9] A. Pantano, G. Modica, and F. Cappello, Mater. Sci. Eng. A **486**, 222 (2008).
[10] Z. Zhou *et al.*, Compos. Sci. Technol. **68**, 1727 (2008).
[11] S. Ogata and Y. Shibutani, Phys. Rev. B **68**, 165409 (2003).
[12] D. Troya, S. L. Mielke, and G. C. Schatz, Chem. Phys. Lett. **382**, 133 (2003).
[13] M. Sammalkorpi *et al.*, Phys. Rev. B **70**, 245416 (2004).
[14] S. L. Zhang *et al.*, Phys. Rev. B **71**, 115403 (2005).
[15] A. Hashimoto *et al.*, Nature (London) **430**, 870 (2004).
[16] K. Suenaga *et al.*, Nature Nanotech. **2**, 358 (2007).
[17] E. J. Seldin and C. W. Nezbeda, J. Appl. Phys. **41**, 3389 (1970).
[18] T. Tanabe, Phys. Scr. **T64**, 7 (1996).
[19] E. Salonen, A. V. Krasheninnikov, and K. Nordlund, Nucl. Instrum. Methods Phys. Res., Sect. B **193**, 603 (2002).
[20] A. V. Krasheninnikov and K. Nordlund, Nucl. Instrum. Methods Phys. Res., Sect. B **228**, 21 (2005).
[21] A. Kis, J. Brugger, and L. Forro *et al.*, Nature Mater. **3**, 153 (2004).
[22] M. Huhtala *et al.*, Phys. Rev. B **70**, 045404 (2004).
[23] S. K. Pregler and S. B. Sinnott, Phys. Rev. B **73**, 224106 (2006).
[24] Z. H. Xia, P. R. Guduru, and W. A. Curtin, Phys. Rev. Lett. **98**, 245501 (2007).
[25] Y. Hirai *et al.*, Jpn. J. Appl. Phys. **42**, 4120 (2003).
[26] S. Xiao and W. Hou, Phys. Rev. B **73**, 115406 (2006).
[27] B. Ashrafi and P. Hubert, Compos. Sci. Technol. **66**, 387 (2006).
[28] A. H. Barber, Appl. Phys. Lett. **87**, 203106 (2005).
[29] A. H. Barber *et al.*, Compos. Sci. Technol. **65**, 2380 (2005).
[30] B. Peng *et al.*, Nature Nanotech. **3**, 626 (2008).
[31] M. F. Yu *et al.*, Science **287**, 637 (2000).
[32] M. F. Yu *et al.*, Phys. Rev. Lett. **84**, 5552 (2000).
[33] This definition differs by factor of $\frac{1}{2}$ from definition used in Ref. [28], but more accurately represents the area fraction of interwall bonds.
[34] D. W. Brenner *et al.*, J. Phys. Condens. Matter **14**, 783 (2002).
[35] O. A. Shenderova *et al.*, Phys. Rev. B **61**, 3877 (2000).
[36] L. A. Girifalco, M. Hodak, and R. S. Lee, Phys. Rev. B **62**, 13 104 (2000).
[37] Z. H. Xia and W. A. Curtin, Phys. Rev. B **69**, 233408 (2004).
[38] H. J. C. Berendsen *et al.*, J. Chem. Phys. **81**, 3684 (1984).
[39] J. W. Hutchinson and Z. Suo, Adv. Appl. Mech. **29**, 63 (1991).
[40] J. M. Hedgepeth and P. Van Dyke, J. Compos. Mater. **1**, 294 (1967).
[41] S. Mahesh and S. L. Phoenix, Int. J. Fract. **127**, 303 (2004).
[42] T. Okabe and M. Nishikawa, J. Mater. Sci. **44**, 331 (2009).
[43] W. Weibull, J. Appl. Mech. **19**, 293 (1951).
[44] W. A. Curtin, Adv. Appl. Mech. **36**, 163 (1999).
[45] J. N. Coleman, Carbon **44**, 1624 (2006).
[46] A. Gard and S. B. Sinnott, Chem. Phys. Lett. **295**, 273 (1998).